

Late-time ensembles of quantum states in quantum chaotic systems

Souradeep Ghosh,¹ Christopher M. Langlett,¹ Nicholas Hunter-Jones,² and Joaquin F. Rodriguez-Nieva¹

¹*Department of Physics & Astronomy, Texas A&M University, College Station, TX 77843*

²*Department of Physics and Department of Computer Science,
University of Texas at Austin, Austin, TX 78712*

Quantum states undergoing quantum chaotic dynamics are expected to evolve into featureless states at late times. While this expectation holds true on an average, coarse-grained level, it is unclear if this expectation applies to higher statistical moments, as symmetries typically present in physical systems constrain the exploration of phase space. Here we study the universal structure of late-time ensembles obtained from unitary dynamics in quantum chaotic systems with symmetries, such as charge or energy conservation. We identify two limiting universal regimes depending on the initial condition. When the initial state is typical—all the moments of the symmetry operators are equal to those of pure random states—then the late-time ensemble is indistinguishable from the Haar ensemble in the thermodynamic limit and at the level of higher statistical moments. Otherwise, atypical initial states evolve into non-universal ensembles which can be distinguished from the Haar ensemble from simple measurements or subsystem properties. Interestingly, such atypical initial conditions are not rare, even when considering product state initial conditions, and can be found in the middle of the spectrum of Hamiltonians known to be ‘maximally’ chaotic. In the limiting case of initial states with negligible variance of the symmetry operator (e.g., states with fixed particle number or states with negligible energy variance), the late-time ensemble has universal behavior captured by constrained RMT ensembles. Our work shows that even though midspectrum states do not explore ergodically all of phase space at late times, the late-time ensemble typically—but not always—exhibits the same average and sample-to-sample fluctuations as the Haar ensemble.

I. INTRODUCTION

The notions of chaos and ergodicity are the two main pillars in the theory of statistical mechanics. In classical many-body systems, chaotic evolution resulting from system nonlinearities leads to repulsion between classical trajectories and ergodic exploration of phase space. This allows us to replace temporal averages by ensemble averages over states compatible with macroscopic constraints, such as energy or particle number. Although defining notions of chaos and ergodicity in quantum regimes has been a long-standing challenge [1–6], as quantum evolution is linear and unitary, in quantum statistical mechanics we draw from our classical intuition to replace temporal averages at late times with averages over all states compatible with the macroscopic constraints [7, 8]. In energy conserving systems, the Gibbs ensemble $\rho = e^{-\beta H}/\text{Tr}[e^{-\beta H}]$ results from finding the most entropic ensemble compatible with the total energy of the system, with the diagonal structure arising from the random phase approximation which accounts for the effect of quantum state averaging. A high energy (or ‘midspectrum’) initial condition will then give rise to a late-time ensemble where the temporal average of an observable is equal to its average over all states in phase space.

However, when describing the late-time behavior of quantum states, there are three subtleties that need to be taken into consideration. First, quantum states in physical quantum systems do not explore the entire phase space even at infinitely long times, as symmetries present in typical physical systems constrain dynamics. For instance, quantum states evolving under

Hamiltonian (or energy conserving) dynamics, $|\Psi\rangle = \sum_{n=1}^D e^{-iE_n t} \langle n|\Psi_0\rangle |n\rangle$, have $D = \dim[\mathcal{H}]$ constraints (\mathcal{H} : Hilbert space) defined by the projection of the initial condition $|\Psi_0\rangle$ on the eigenstate basis $|n\rangle$. In this case, quantum states evolve on a high-dimensional torus with amplitudes $|\langle n|\Psi_0\rangle|$, rather than on the full Hilbert space. For this reason, a pertinent question to ask is whether the lack of phase space ergodicity has any measurable fingerprint in the late-time behavior of quantum states.

Second, the late time behavior of quantum states depends on the choice of the initial condition $|\Psi_0\rangle$, which determines the statistical properties of quantum states at late times from the onset of dynamics. For this reason, it is unclear whether it is possible to make universal statements about the statistical properties of quantum state at late times that are independent of $|\Psi_0\rangle$, particularly at the level of higher statistical moments, and beyond the average behavior already captured by the Gibbs ensemble.

Third, the timescales in which states explore uniformly all of the available phase space are relatively long. In particular, temporal averages need to be done over timescales proportional to the available Hilbert space in order capture all the statistical moments of the late-time ensemble. That is, a midspectrum initial condition will take exponentially long times to explore all of phase space. Such timescales are beyond the reach of existing experimental platforms. If we allow the sampling timescales to be made arbitrarily large, then the ensemble of states at late times has been shown [9] to be equivalent to *random phase ensemble* [10, 11], defined as the ensemble of states spanned by $|\Psi\rangle = \sum_{n=1}^D e^{i\theta_n} |\langle n|\Psi_0\rangle| |n\rangle$ with θ_n a random phase. This result is true so long as

the Hamiltonian satisfies a no- k resonance condition to all k -orders.

These questions are very relevant for today's experiments with programmable quantum platforms, such as systems comprised of superconducting qubits [12–14], Rydberg atoms [15–17], or trapped ions [18, 19]. Such systems can retrieve extremely detailed statistical information about quantum states through their ability to take microscopically-resolved measurements of individual degrees of freedom, and the ability to evolve states with high precision and repetition rate. From such measurements one can retrieve the full distribution of outcome probabilities of a microscopic observable [20–22] or the subsystem entanglement entropy [23–26], both of which are sensitive to the fine-grained structure of quantum states. These capabilities are qualitative distinct from more traditional thermodynamic or transport probes, which typically measure coarse-grained observables (i.e., long wavelength and low frequency) such that higher statistical moments are averaged out.

Given these modern experimental capabilities, in recent years there has been intense theoretical activity aiming to understand chaos and ergodicity beyond the coarse-grained behavior described by RMT [27]. In particular, our current understanding of quantum chaos and ergodicity is rooted in the RMT behavior of eigensystem properties, such as the behavior of the level spacing statistics [28–30] or the spectral form factor [31–34], and the volume-law behavior of eigenstate entanglement entropy (EE) [35–39]. Recent efforts have aimed to go beyond these coarse features to capture 'fine' feature of quantum thermalization, such as how spatial locality is imprinted in the structure of quantum states [40–43], and how this structure gives rise to fine features in the level spacing statistics, the matrix elements of local observables, or between eigenstates [44–49]. Other works [50–54] have aimed to quantify randomness of quantum state ensembles at the level of higher statistical moments using k -designs [55, 56]. Many other statistical approaches are being developed to capture higher-order fluctuations of matrix elements of local observables [57–59].

In this work we focus on the question of universality of the late-time ensemble at the level of higher statistical moments, in terms of the sensitivity of the late time ensemble to the choice of the initial condition, and how the lack of ergodicity affects the statistical properties of quantum states at late times. Specifically, we consider the late-time dynamics of initial product states (i.e., low entanglement states) lying in the middle of the spectrum of quantum chaotic systems, and assume that states can be sampled at arbitrarily long times. Although such states are expected to evolve into featureless states at late times, we show that this expectation only applies to their coarse-grained features, such as the volume-law behavior of the entanglement entropy. In contrast, here we identify much richer dynamical behaviors when looking at the higher statistical moments of the late-time ensemble. In particular, for quantum chaotic systems with spatial lo-

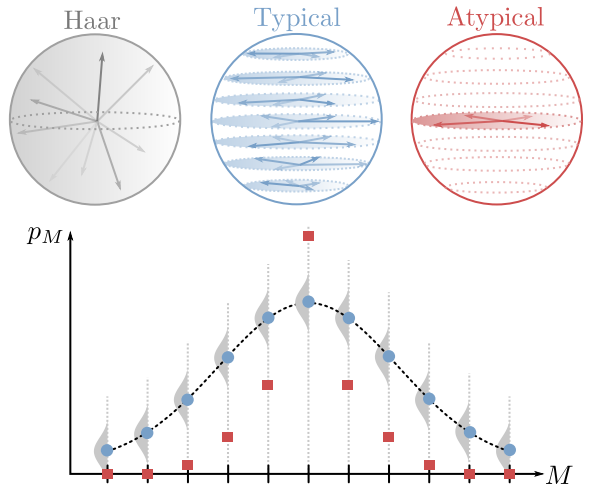


FIG. 1. The late-time behavior of an initial state $|\Psi_0\rangle$ can be classified by its distribution of outcome probabilities of the symmetry operator $O = \sum_n O_n |n\rangle\langle n|$ relative to that produced by the ensemble of Haar random states. A typical initial state has the same distribution of outcome probabilities as pure random states. In contrast, an atypical initial state has a distribution which has smaller than typical fluctuations of the symmetry operator. Schematics for typical and atypical states are shown for a magnetic charge $O = \sum_i Z_i$ with quantum number M .

cality and energy conservation as their only features, we show that there exist two limiting late-time regimes with distinct universal properties which depend on the choice of initial condition. The key results of the present work are as follows.

A. Summary of key results

We focus on the statistical properties of quantum state ensembles at *late-times* generated by a unitary evolution operator \hat{U}_t . The late-time ensemble is defined as

$$\Phi_{T \rightarrow \infty} = \left\{ |\Psi_i\rangle = \hat{U}_{t_i} |\Psi_0\rangle, t_i \in [T, \infty] \right\}, \quad (1)$$

where the states $|\Psi_i\rangle$ are drawn randomly at times t_i after a long initial time $T \gg 1$ has passed. We focus on quantum chaotic dynamics constrained by a symmetry \hat{O} describing a local scalar charge, such as particle number or energy. Specifically, we ask whether the constraint introduced by \hat{O} gives rise to distinguishable features relative to pure random states that can be measured from subsystem properties or simple observables.

The late-time behavior of $|\Psi_0\rangle$ can be characterized in terms of the distribution of outcome probabilities of the symmetry operator \hat{O} (Fig. 1). First, we perform a spectral decomposition of the operator \hat{O} , which takes the form, $\hat{O} = \sum_n O_n |n\rangle\langle n|$, with $|n\rangle$ the eigenvectors of \hat{O} and O_n its eigenvalues. The initial state $|\Psi_0\rangle$ gives rise to a probability distribution $f(O)$ which can be expressed

in the eigenbasis of the operator \hat{O} as

$$f(O) = \sum_n |\langle n | \Psi_0 \rangle|^2 \delta(O - O_n). \quad (2)$$

All the moments of $f(O)$ are preserved during the evolution, as each factor $f_n = |\langle n | \Psi_0 \rangle|^2$ remains constant during evolution. Similarly, the Haar ensemble Φ_{Haar} of pure random states in the full Hilbert space \mathcal{H} generates a reference distribution

$$g(O) = \sum_n \langle |\langle n | \Psi \rangle|^2 \rangle \delta(O - O_n), \quad (3)$$

where the outer brackets denote average over Haar random states, $\langle [\dots] \rangle = \int \prod_\sigma d\Psi_\sigma d\bar{\Psi}_\sigma [\dots] \delta(|\Psi|^2 - 1)$. Due to randomness of $|\Psi\rangle$, each value of $g_n = \langle |\langle n | \Psi \rangle|^2 \rangle = 1/D$ is uniformly distributed, with $D = \dim[\mathcal{H}]$.

We say that an initial state is *typical* if it satisfies the condition

$$f(O) = g(O), \quad (4)$$

i.e., all the moments for the outcome distribution of the operator O are equal between the initial state and Haar random states (see Fig. 1). Simple initial states which are typical are not hard to prepare in experiments, as product states of spin with random orientations usually spread rather uniformly across the eigenbasis of \hat{O} for symmetries such as charge or energy conservation. If the system exhibits additional symmetries, the condition (4) needs to apply for each symmetry operator. For typical initial states, we find that the late-time ensemble and the Haar ensemble share exactly the same finite k -moments in the thermodynamic limit, even though the time-evolved states do not explore the entire Hilbert space. In other words, there is no measurement that one can do at the level of finite statistical moments to tell that states are not exploring the entire Hilbert space. In the case of finite-sized systems, it is exponentially hard to distinguish the late-time ensemble from the Haar ensemble. For instance, when considering subsystem entropies, the late-time ensemble of a typical initial state has an average entanglement entropy equal to the Page entropy [60] up to, possibly, exponentially-small-in-subsystem corrections. The reason behind this behavior is that, although symmetries constrain evolution and not all states are explored at late times, typical initial conditions efficiently mix all symmetry sectors at the onset of quantum evolution and give rise to Haar-like moments at late times. We show that this behavior is robust across families of chaotic Hamiltonians.

If the distributions $f(O)$ and $g(O)$ disagree (Fig. 1), i.e. the initial state is *atypical*, then the late-time ensemble is distinguishable from the Haar ensemble at the level of the first moment, and such differences can be detected from subsystem properties or from simple local measurements. A main focus of the present work is when the first moment of $f(O)$ and $g(O)$ agree but higher moments do

not. In this case, the initial state is a midspectrum initial state, but its fluctuations are atypical. As we will see, this leads to deviations from pure random states which are nonuniversal and depend on details of $f(O)$. We show that atypical states are not rare, even when considering product state initial conditions, and can be easily be found even in the middle of the spectrum of strongly chaotic Hamiltonians.

In the limiting case of initial conditions with negligible variance of the symmetry operator, such as states with fixed particle number or energy negligible variance, the late-time ensemble acquires universal behavior described by constrained RMT ensembles. In essence, such ensembles are Haar random states constrained to a specific sector of the symmetry operator, i.e., they capture the microcanonical properties of the symmetry operator. Such constrained RMT ensembles have lower entropy (and thus more structure) than pure random states. As will be shown below, and also shown in Ref. [42], the microcanonical ensemble for quantum chaotic Hamiltonians exhibit a much richer landscape of behaviors as a function of model parameters, and acquire universal behavior in ‘maximally chaotic’ regions of parameter space. This is in contrast to late-time ensemble of typical initial states which converge to behavior of the Haar ensemble irrespective of model parameters.

The outline for the rest of the work is as follows. In Sec. II, we use a simple analytically-tractable model to prove that constrained ensembles that satisfy the typicality condition are indistinguishable from Haar random states at the level of finite k moments and in the thermodynamic limit. In Sec. III, we focus on the statistical properties of subsystem properties, particularly the von Neumann entanglement entropy, and review the relevant distributions for constrained and unconstrained RMT ensembles relevant to our work. In Sec. IV, we show numerical results for random quantum circuits in the presence of a U(1) scalar charge. In Sec. V we extend the numerical results to local chaotic Hamiltonian systems, showing that the same conclusions obtained in Sec. II apply to more generic quantum chaotic systems. In Sec. VI we summarize the main results and discuss their ramifications.

II. MOMENTS OF CONSTRAINED QUANTUM STATE ENSEMBLES: EXACT RESULTS

We now prove the main results of the present work in a simple and analytically-tractable model, namely, ensembles of pure random states in the presence of a U(1) constraint. Let us consider a chain of L spin-1/2 qubits with total Hilbert space dimension $D = 2^L$. We factor the Hilbert space into $(L+1)$ magnetic sectors of the symmetry operator $\hat{Z} = \sum_i^L \hat{Z}_i$, with M ($0 \leq M \leq L$) labelling the total number of spins down in a given sector. Each magnetic sector has Hilbert space dimension $D_M = \binom{L}{M}$, with $\sum_{M=0}^L D_M = D$.

Let us now draw pure random states from the ensemble defined as

$$|\Phi\rangle = \sum_{M=0}^L \sqrt{p_M} |\Phi_M\rangle, \quad (5)$$

where $p_M = D_M/D$ is fixed, and $|\Phi_M\rangle \in \mathcal{H}(M)$ are normalized random states within the subspace with fixed M particles, $|\Phi_M\rangle = \sum_{\alpha=1}^{D_M} \phi_{M,\alpha} |M, \alpha\rangle$, with $\sum_{\alpha=1}^{D_M} |\phi_{M,\alpha}|^2 = 1$ and α labeling the states within the sector M . We first note that states drawn from Eq. (5) are typical, as pure random states drawn from the Haar ensemble also have projection $\sum_i p_i \langle \Psi_i | \hat{P}_M | \Psi_i \rangle = p_M$ in each symmetry sector with quantum number M (here \hat{P}_M denotes the projection operator on the magnetic sector M , $\hat{P}_M = \sum_{\alpha=1}^{D_M} |M, \alpha\rangle \langle M, \alpha|$). We also note that $\sum_M p_M = 1$, so the states $|\Phi\rangle$ are properly normalized.

Because the values of p_M are fixed, the ensemble Φ in Eq. (5) does not explore the entire Hilbert space. For instance, the states $|\uparrow\uparrow\ldots\uparrow\rangle$ and $|\uparrow\downarrow\ldots\uparrow\rangle$ are not part of Φ . Nevertheless, we will see that Φ and the Haar ensemble are indistinguishable for all finite k and in the thermodynamic limit. In the case of finite-sized systems, differences between finite moments are $\mathcal{O}(1/D)$ and, therefore, hard to measure. Before proving the previous statement, we first review some basics of ensemble averaging.

A. Ensemble of Haar Random States

Let us consider pure random states in a Hilbert space of dimension D , $|\Psi\rangle = \sum_{n=1}^D \psi_n |n\rangle$. One can think of $|\Psi\rangle$ as a D -dimensional vector of randomly distributed Gaussian variables which are not independent as they must satisfy the normalization condition, $\sum_{n=1}^D |\psi_n|^2 = 1$. The k -th moment of the Haar ensemble is defined in terms of the $D^k \times D^k$ density matrix obtained by averaging k copies of the state $|\Psi\rangle$:

$$\rho^{(k)} = \underbrace{\langle |\Psi\rangle \langle \Psi| \otimes \dots \otimes |\Psi\rangle \langle \Psi|}_{k \text{ copies}}. \quad (6)$$

For example, the first moment of the distribution is

$$\rho_{m,n}^{(k=1)} = \langle \psi_m \bar{\psi}_n \rangle = \frac{\delta_{m,n}}{D}. \quad (7)$$

This equality can be obtained from taking ensemble average over the normalization condition $\sum_n \langle \psi_n \bar{\psi}_n \rangle = 1$, and noting that all the components of the wavefunction are equivalent, which results in each of the wavefunction's component having variance $1/D$. In addition, ensemble average over distinct components gives zero, as each component is uncorrelated.

The second moment of the Haar ensemble is

$$\begin{aligned} \rho_{m_1 m_2, n_1 n_2}^{(k=2)} &= \langle \psi_{m_1} \bar{\psi}_{n_1} \psi_{m_2} \bar{\psi}_{n_2} \rangle \\ &= \frac{\delta_{m_1, n_1} \delta_{m_2, n_2} + \delta_{m_1, n_2} \delta_{m_2, n_1}}{D(D+1)}. \end{aligned} \quad (8)$$

Similarly to the $k = 1$ case, this result can be obtained from taking ensemble average of the square of the normalization condition $\sum_{n,n'} \langle \psi_n \bar{\psi}_n \psi_{n'} \bar{\psi}_{n'} \rangle = 1$, which contains $D(D-1)$ equivalent terms with $n \neq n'$, and D terms with $n = n'$ which contribute twice to the summation (as there are two ways to contract the Gaussian variables). This gives rise to a total of $D(D+1)$ equivalent terms that sum to 1.

More generally, one can prove [61] that

$$\rho_{\vec{m}, \vec{n}}^{(k)} = \langle \prod_{i=1}^k \psi_{m_i} \bar{\psi}_{n_i} \rangle = \frac{\sum_{\vec{\sigma} \in P_k} \delta_{\vec{m}, P_{\vec{\sigma}}(\vec{n})}}{\prod_{j=0}^{k-1} (D+j)}, \quad (9)$$

where $\vec{m} = (m_1, \dots, m_k)$ and $\vec{n} = (n_1, \dots, n_k)$ denotes vectors labeling the entries of the $D^k \times D^k$ matrix in the basis $|n\rangle$, $P_{\vec{\sigma}}(\vec{n})$ denotes permuting the indices of the vector \vec{n} for all possible permutations $\vec{\sigma}$ of k indices, and $\delta_{\vec{n}, \vec{m}}$ is a short-hand notation for $\delta_{\vec{n}, \vec{m}} = \delta_{n_1, m_1} \delta_{n_2, m_2} \dots \delta_{n_k, m_k}$. Haar moments of this form are equivalently projectors on to the symmetric subspace of k copies of the Hilbert space.

From Eq. (9) we see that, when we consider finite moments of the distribution in the thermodynamic limit $D \rightarrow \infty$, it is legitimate to replace Eq. (9) by

$$\rho_{\vec{m}, \vec{n}}^{(k)} = \langle \prod_{i=1}^k \psi_{m_i} \bar{\psi}_{n_i} \rangle \approx \frac{\sum_{\vec{\sigma} \in P_k} \delta_{\vec{m}, P_{\vec{\sigma}}(\vec{n})}}{D^k}, \quad (10)$$

where $\mathcal{O}(1)$ terms are neglected relative to D . This is exactly the same result that one would get for an unnormalized random vector with D independent random gaussian variables.

B. Ensemble of Typical Random States

Let us now compute the first few moments of the distribution $|\Phi\rangle$ in Eq. (5). Here we label states in the eigenbasis of the \hat{Z} operator, $m = (M, \alpha)$, with $1 \leq \alpha \leq D_M$. The first moment of the ensemble Φ is

$$\begin{aligned} \rho_{(M\alpha), (N\beta)}^{(k=1)} &= \sqrt{p_M p_N} \langle \phi_{M\alpha} \bar{\phi}_{N\beta} \rangle \\ &= p_M \frac{\delta_{M\alpha, N\beta}}{D_M} = \frac{\delta_{n,m}}{D}, \end{aligned} \quad (11)$$

where in the third equality we used $p_M = D_M/D$ combined with Eq. (7) applied to pure random states within the symmetry sector with quantum number M . In the last equality in (11) we relabelled the states as $|n\rangle = |M\alpha\rangle$. Equation (11) agrees *exactly* with Eq. (7), thus the ensemble of Haar random states and the ensemble of typical states have the same first moment.

Calculation of the $k = 2$ moment of the ensemble Φ is somewhat more complicated and needs to be separated into two different cases: (i) $M_1 \neq M_2$, and (ii) $M_1 = M_2$.

In the case $M_1 \neq M_2$, we find

$$\begin{aligned}\rho_{\vec{M}\vec{\alpha},\vec{N}\vec{\beta}}^{(k=2)} &= \sqrt{p_{M_1}p_{N_1}p_{M_2}p_{N_2}}\langle\phi_{M_1\alpha_1}\bar{\phi}_{N_1\beta_1}\phi_{M_2\alpha_2}\bar{\phi}_{N_2\beta_2}\rangle \\ &= p_{M_1}p_{M_2}\frac{\delta_{M_1\alpha_1,N_1\beta_1}\delta_{M_2\alpha_2,N_2\beta_2} + (N_1\beta_1 \rightleftharpoons N_2\beta_2)}{D_{M_1}D_{M_2}} \\ &= \frac{\delta_{m_1,n_1}\delta_{m_2,n_2} + \delta_{m_1,n_2}\delta_{m_2,n_1}}{D^2}.\end{aligned}\quad (12)$$

In the case $M_1 = M_2$, we find

$$\begin{aligned}\rho_{\vec{M}\vec{\alpha},\vec{N}\vec{\beta}}^{(k=2)} &= p_{M_1}^2\frac{\delta_{M_1\alpha_1,N_1\beta_1}\delta_{M_1\alpha_2,N_2\beta_2} + (N_1\beta_1 \rightleftharpoons N_2\beta_2)}{D_{M_1}(D_{M_1} + 1)} \\ &= \frac{\delta_{m_1,n_1}\delta_{m_2,n_2} + (n_1 \rightleftharpoons n_2)}{D^2(1 + D_{M_1}^{-1})}.\end{aligned}\quad (13)$$

Unlike the first moment, the second moment of the ensemble of typical states does not agree exactly with the second moment of the ensemble of Haar random states, Eq. (7). To quantitatively estimate the difference between the second moments, we first compute the difference $\delta\rho^{(k)}$ between the matrices $\rho_{\vec{m},\vec{n}}^{(k=2)}$ for Haar random states and typical random states, and then compute its trace distance Δ_k . The trace distance of a matrix is defined as the half sum of the absolute values of its eigenvalues. When the trace distance is computed on the difference between two density matrices, each of which has a trace equal to one, the minimum value of Δ_k is 0 (when the density matrices are equal) and its maximum value is 1. As shown in the Appendix, the trace distance $\Delta_{k=2}$ between ensembles is given by

$$\Delta_{k=2} = \frac{1}{D} \left(1 - \frac{1}{\sqrt{\pi L}} \right) + \mathcal{O}\left(\frac{1}{D^2}\right), \quad (14)$$

which is exponentially small in system size, and goes to zero in the thermodynamic limit.

For higher moments, $k > 2$, we take a shortcut and start the calculation by assuming $D \rightarrow \infty$. In this case, we can use the analogue of Eq. (10) for each symmetry sector M and assume that each D_M -dimensional vector $\phi_{M,\alpha}$ has random and independently-distributed components with variance $1/D_M$ (i.e., no normalization constraint). Then, the k -th moment of the ensemble Φ in the thermodynamic limit is

$$\begin{aligned}\rho_{(\vec{M}\vec{\alpha}),(\vec{N}\vec{\beta})}^{(k)} &= \sqrt{p_{M_1}p_{N_1}\dots p_{M_k}p_{N_k}}\langle\prod_{i=1}^k\phi_{M_i\alpha_i}\bar{\phi}_{N_i\beta_i}\rangle \\ &= p_{M_1}\dots p_{M_k}\frac{\sum_{\vec{\sigma}\in P_k}\delta_{\vec{M}\vec{\alpha},P_{\vec{\sigma}}(\vec{N}\vec{\beta})}}{D_{M_1}\dots D_{M_k}} \\ &= \frac{\sum_{\vec{\sigma}\in P_k}\delta_{\vec{m},P_{\vec{\sigma}}(\vec{n})}}{D^k}.\end{aligned}\quad (15)$$

In this case, Eq. (15) agrees *exactly* with Eq. (10) for all finite k and in the thermodynamic limit.

C. Ensemble of Atypical Random States

For the sake of completeness, let us now consider the microcanonical ensemble of pure random states constrained to the largest symmetry sector ($M_0 = L/2$) of the \hat{Z} operator,

$$|\Phi_{M_0}\rangle = \sum_{\alpha=1}^{D_{M_0}}\phi_{M_0,\alpha}|M_0,\alpha\rangle. \quad (16)$$

The first moment of the ensemble of Φ' is given by

$$\rho_{M\alpha,N\beta}^{(k=1)} = \delta_{M,M_0}\langle\phi_{M,\alpha}\bar{\phi}_{N,\beta}\rangle = \delta_{M,M_0}\frac{\delta_{M\alpha,N\beta}}{D_{M_0}}, \quad (17)$$

which already differs from the first moment of the Haar ensemble, Eq. (7). In this case, the trace distance between the first moment of the Haar ensemble and the ensemble Φ' is given by

$$\Delta_{k=1} = \left(1 - \sqrt{\frac{2}{\pi L}}\right), \quad (18)$$

which is nearly the maximal distance between the two ensembles. As shown below, such differences are measurable from subsystem properties.

III. MOMENTS OF ENTANGLEMENT ENTROPY WITHIN ENSEMBLES

In this section we focus on subsystem properties of the quantum state ensembles, which are easier to probe in experiments. In essence, the question we aim to address below is whether the lack of phase space ergodicity discussed in the previous section can be diagnosed from the statistics of local observables (i.e., without access to the full quantum state). In particular, here we consider the distribution of the von Neumann entanglement entropy (EE),

$$S_A = -\text{Tr}[\rho_A \log(\rho_A)], \quad (19)$$

at late times [62–65], specifically timescales after which the ‘linear ramp’ behavior has passed [66, 67]. In Eq. (19), $\rho_A = \text{Tr}_B[|\Psi_i\rangle\langle\Psi_i|]$ is the reduced density matrix of the state $|\Psi_i\rangle \in \Phi$ ($\Phi = \Phi_{\text{Haar}}$ or Φ_M) when the system is bipartitioned into two subsystems of length $L_A = fL$ and $L_B = (1-f)L$, with L the number of qudits in a system with local Hilbert space dimension d . The numerical results below will be specifically for the half-system EE, $f = 1/2$, but in this section we discuss the entanglement behavior for arbitrary f .

There are several advantages of looking into the statistical properties of half-system EEs. First, the distribution of EE is known for various classes of constrained [39, 68] and unconstrained [68–70] ensembles of

pure random states, which we briefly review below. Second, if the distribution of half-system EE is indistinguishable from that of Haar random states, then the same is true for $L_A < L/2$. This is because the subsystem A is coupled to a larger bath the smaller the value of L_A , thus the state ρ_A is ‘more thermal’. We now briefly review the behavior for the first and second moments of the EE for constrained and unconstrained ensembles relevant to our work. In particular, we will focus on the *asymptotic* behavior of the EE distributions, and refer the reader to the exact analytical expressions in Refs. [39, 68–70].

A. Entanglement patterns for the Haar ensemble

In the absence of any structure, the distribution of EE of pure random states drawn from Φ_{Haar} depends only on subsystem dimensions through the parameters f and L . The average EE is given by

$$\mu_H \approx Lf \log d - \frac{1}{2}\delta_{f,1/2}, \quad (20)$$

which was first conjectured by Page [60] and later proven analytically by others [68–70]. The first term in the RHS of Eq. (20) is the volume-law term which scales with subsystem size $L_A = fL$, and the second term gives rise to the ‘half-qubit’ shift correction for half subsystems. The variance of EE for pure random states, $\sigma_H^2 \approx d^{-L(1+|1-2f|)}$, is exponentially small in subsystem size. This implies that the EE is typical and a single pure random state has the Page entropy in Eq. (20).

B. Entanglement patterns for constrained ensembles: U(1) and energy conserving systems

For systems with a local scalar charge (particle number or energy) and a local Hilbert space dimension of $d = 2$, it is convenient to think of $0 \leq M \leq L$ as an integer charge number, and each site able to accommodate a maximum of one charge only. This is exactly true for conservation of particle number or magnetization, but only an approximation in energy conserving systems. The Hilbert space $\mathcal{H}(M)$ of states with fixed charge M decomposes as a direct sum of tensor products,

$$\mathcal{H}(M) = \bigoplus_{M_A} \mathcal{H}_A(M_A) \otimes \mathcal{H}_B(M - M_A), \quad (21)$$

where M_A is an integer number varying within the range $\max(0, M - L_B) \leq M_A \leq \min(M, L_A)$. The Hilbert space dimension of $\mathcal{H}_A(M_A)$ is $d_{A,M_A} = \binom{L_A}{M_A}$, the Hilbert space dimension of $\mathcal{H}_B(M - M_A)$ is $d_{B,M-M_A} = \binom{L-L_A}{M-M_A}$, and the total Hilbert space dimension is $\sum_{M_A} d_{A,M_A} d_{B,M-M_A} = d_M = \binom{L}{M}$. A random state within a fixed charge sector $|\Phi_M\rangle \in \mathcal{H}(M)$ can be expressed as a superposition of orthonormal basis states,

$|\Phi_M\rangle = \sum_{M_A} \phi_{\alpha,\beta}^{(M_A)} |M_A, \alpha\rangle \otimes |M - M_A, \beta\rangle$, with $\phi_{\alpha,\beta}^{(M_A)}$ uncorrelated random numbers up to normalization. The index α (β) labels the basis states in subsystem A (B) with a total charge M_A ($M - M_A$).

The reduced density matrix of subsystem A is block diagonal, $\rho_A = \text{Tr}_B[|\Phi_M\rangle\langle\Phi_M|] = \sum_{M_A} p_{M_A} \rho_{A|M_A}$, where $\rho_{A|M}$ denotes the block with M_A particles, and the factors $p_{M_A} \geq 0$ are the (classical) probability distribution of finding M_A particles in A . The entanglement entropy can be written as $S(\rho_A) = \sum_{M_A} p_{M_A} S(\rho_{A|M_A}) - p_{M_A} \log p_{M_A}$, where the second term on the RHS is the Shannon entropy of the number distribution p_{M_A} , which captures particle number correlations between the two subsystems, and the first term captures quantum correlations between configurations with a fixed particle number.

The first few moments of the EE distribution produced by $|\Phi_M\rangle \in \mathcal{H}(M)$ was first computed in Ref. [68]. The mean entanglement entropy for ‘mid-spectrum’ states (i.e., $M/L = 1/2$) in the asymptotic limit is given by

$$\mu_M = Lf \log(d) + \frac{f + \log(1-f)}{2} - \frac{1}{2}\delta_{f,1/2}. \quad (22)$$

Interestingly, in addition to the volume-law term and the half-qubit shift, Eq. (22) also exhibits a finite shift in the mean EE entropy relative to the Haar result in Eq. (7). The variance of EE scales exponentially with system size, $\sigma_M \sim \sqrt{L}/d^L$, thus a typical pure random state in $\mathcal{H}(M)$ will have the EE in Eq. (22). We emphasize that the differences between the average EE in Eqs. (20) and (22) are significant on the exponentially small scale set by σ_M .

Although the above analysis is valid exactly for systems with a U(1) scalar charge, in Refs. [42, 43] we argued that the EE distribution of the microcanonical eigenstate ensemble (i.e., the analogue of states with zero magnetization variance) in local Hamiltonian systems has the same asymptotic behavior as that in systems with a U(1) scalar charge.¹ Specifically, the correspondence between ensembles of Hamiltonian eigenstates and constrained RMT ensembles was shown to hold in regions of Hamiltonian parameter space where eigenstates behave as ‘maximally chaotic’. In these regions, eigenstates are maximally entropic and only ‘know’ about spatial locality and energy conservation, while the remaining non-universal microscopic features are washed away. Below we discuss the eigenstate ensembles generated both by ‘maximally chaotic’ Hamiltonians and Hamiltonians per-

¹ The Hilbert space of local Hamiltonian systems cannot be factored out as in Eq. (21) because the energy operator in local systems is typically written as a sum of 2-local operators and the energy spectrum is distributed continuously; however, one can think of the U(1) constrained ensemble Φ_M as the asymptotic ensemble to which systems with one local scalar charge converge to, as all the non-universal microscopic differences between systems with a local scalar charge are washed away when the subsystem dimension is $d_A \gg 1$.

turbed away from maximal chaos, and show that they exhibit important differences with respect to the late-time ensembles generated by dynamics.

IV. ENSEMBLES EMERGING FROM U(1) RANDOM QUANTUM CIRCUITS

A. Model

To illustrate the above results in a simple model, we first consider a random quantum circuit model [71] comprised of a one-dimensional chain with L sites and periodic boundary conditions, where each site contains a qubit with local Hilbert space dimension $d = 2$. The time-evolution is constrained to conserve the total z component of the spin-1/2's, $\hat{S}_z = \sum_j \hat{Z}_j$. In particular, we use brickwork circuits with staggered layers of unitary gates with range $r = 2$ [72]. The range r is the number of contiguous qubits each individual gate acts on, so that $\hat{U}_{j,j+1,\dots,j+(r-1)}$ acts on sites $(j, j+1, \dots, j+r-1)$. Each gate is a $d^r \times d^r$ block diagonal matrix, with $(r+1)$ blocks labeled by the total z charge of the qubits on r sites: $\sum_{i=j}^{j+r-1} \hat{Z}_i$. The blocks have size $\binom{r}{n}$ with $n = 0, 1, \dots, r$. In the $r = 2$ case, the gates $\hat{U}_{j,j+1}$ have the structure:

$$\hat{U}_{j,j+1} = \begin{pmatrix} \begin{pmatrix} \uparrow\uparrow \\ U(1) \end{pmatrix} & \begin{pmatrix} \uparrow\downarrow & \downarrow\uparrow \\ U(2) & \end{pmatrix} & \begin{pmatrix} \downarrow\downarrow \\ U(1) \end{pmatrix} \\ & & \end{pmatrix}, \quad (23)$$

comprised of (i) a 1×1 block acting in the $|\uparrow\uparrow\rangle$ subspace, (ii) a 2×2 block acting in the $|\uparrow\downarrow\rangle, |\downarrow\uparrow\rangle$ subspace, and (iii) a 1×1 block acting in the $|\downarrow\downarrow\rangle$ subspace.

At time step t , we first apply a layer of unitary gates $\hat{U}_o(t)$ acting on odd-even sites, followed by a second layer of unitary gates $\hat{U}_e(t)$ acting on even-odd sites:

$$\hat{U}_o(t) = \prod_{j=1}^{L-1} \hat{U}_{j,j+1}(t), \quad \hat{U}_e(t) = \prod_{j=2}^L \hat{U}_{j,j+1}(t). \quad (24)$$

such that the total unitary at time t is $\hat{U}(t) = \hat{U}_o(t')\hat{U}_e(t')$. At each time step, each of the $\hat{U}_{j,j+1}(t)$ gates in Eq. (23) are independently and randomly chosen.

To obtain the late-time ensemble, we compute sequence of states $|\Psi_{t+1}\rangle = \hat{U}_t|\Psi_t\rangle$ starting from the initial condition $|\Psi_0\rangle$. We first apply $t \gg L$ layers of unitary gates to reach thermalization, which we define as the timescale in which the average EE reaches its late-time value (within one standard deviation of the EE at late times). Using $L = 16$, we find that $t = 100$ layers is sufficient to reach thermalization for all the initial conditions used. After thermalization, we draw 1000 states to sample the late-time distribution.

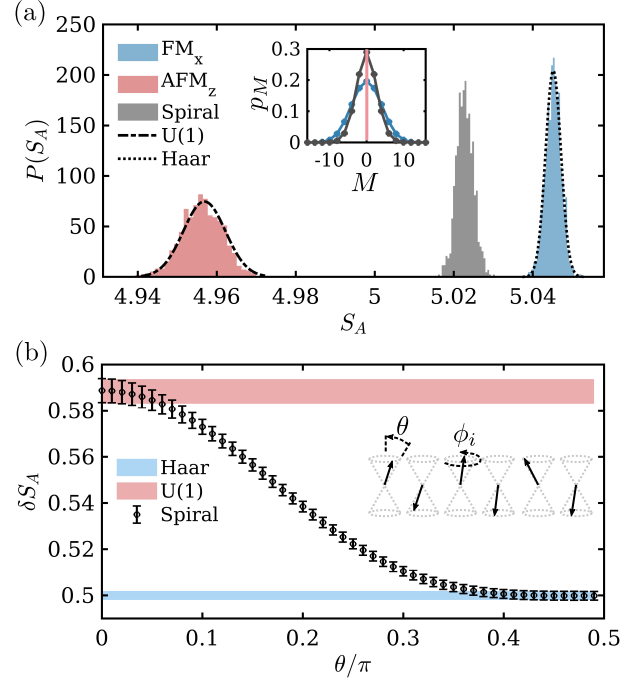


FIG. 2. (a) Distribution of half-system entanglement entropy (EE) at late-times for a random quantum circuit with a U(1) conservation law. All the initial conditions considered have zero average magnetization $\langle \hat{S}_z \rangle = 0$ but different magnetization variance δS_z^2 , ranging from 0 (AFM_z) to $L/4$ (FM_x). Also shown is a generic EE distribution for a spin spiral state, Eq. (27), with $\theta = \pi/4$. The dotted line indicates the exact EE distribution for pure random states (Haar), and the dotted-dashed lines indicates the EE distribution of constrained random states [U(1)] derived in Ref. [68]. The inset shows the projection p_M of the initial condition within symmetry sectors M for each of the initial conditions. (b) Distribution of EE plotted relative to the maximum EE value ($\delta S_A = L_A \log 2 - S_A$) for spin spiral states, Eq.(27), as a function of the canting angle θ .

B. Initial Conditions

We consider two product state initial conditions, the first describing spins aligned in the x direction and the second describing consecutive spins anti-aligned in the z direction:

$$|FM_x\rangle = \frac{1}{\sqrt{2^L}} \bigotimes_{j=1}^L (|\uparrow\rangle_j + |\downarrow\rangle_j), \quad (25)$$

$$|AFM_z\rangle = |\uparrow\downarrow\uparrow\downarrow\dots\downarrow\rangle. \quad (26)$$

Both initial conditions have total magnetization $\langle \hat{S}_z \rangle = 0$. However, the FM_x state has projection on all symmetry sectors M , with $p_M = d_M/2^L$, whereas AFM_z has only projection in the largest $M = L/2$ sector. As such, FM_x in Eq. (25) satisfies the typicality in condition defined in Eq. (4), whereas the AFM_z in Eq. (26) is atypical and has zero magnetization variance.

C. Numerical Results

Figure 2 shows the EE distribution at late times starting from the FM_x and AFM_z initial conditions. Both distributions are distinguishable at the level of subsystem entropies, as the their means are separated by a value much larger than their standard deviations. On the one hand, the FM_x initial condition mixes all symmetry sectors according to the typicality condition, and the resulting EE distribution at late times is indistinguishable from the EE distribution of Haar random states (dotted lines). On the other hand, states obtained from the AFM_z initial condition are restricted to the largest $M = L/2$ sector and agree exactly with the $\text{U}(1)$ constrained distribution derived in Refs. [39, 68]. We emphasize that the differences between distributions are not a finite size effect, but they persist in the thermodynamic limit, c.f., asymptotic behaviors of Eqs. (7) and (11).

As we will show below using other examples, the constrained [$\text{U}(1)$] and unconstrained (Haar) distributions can be interpreted as the two *limiting* universal distributions in generic systems with a local scalar charge. Interestingly, we can also generate any other EE distribution falling in-between these two limiting distributions [e.g., middle histogram in Fig. 2(a)]. To show this, we use an antiferromagnetic spin spiral state defined as

$$|\theta\rangle = \bigotimes_{j=1}^L \left(\cos \theta_j |\uparrow\rangle_j + e^{i\phi_j} \sin \theta_j |\downarrow\rangle_j \right), \quad (27)$$

where the canting angle θ_j is equal to $\theta_j = \theta$ in odd sites, $\theta_j = \theta + \pi$ in even sites, and the azimuthal angle ϕ_j is given by $\phi_j = \frac{2\pi j}{L}$, see inset of Fig. 2(b). By tuning the angle θ , we go from an AFM_z initial condition in Eq. (26) with zero magnetization variance at $\theta = 0$, to product states of spins spiraling in the xy plane with magnetization variance that satisfies the typicality condition at $\theta = \pi/2$.

The EE distribution as a function of θ is shown in Fig. 2(b). Each datapoint represents the mean EE of the distribution, the bars indicate its standard deviation, and the EE is plotted relative to its maximum value ($\delta S_A = L_A \log 2 - S_A$). As anticipated, we find that the EE distribution at late times can fall anywhere in between that of Φ_{Haar} or $\Phi_{\text{U}(1)}$ by tuning the value of θ between $0 < \theta < \pi/2$. In the next section, we will show that the same behavior also applies to more generic situations describing local Hamiltonian systems where the charge is continuously distributed.

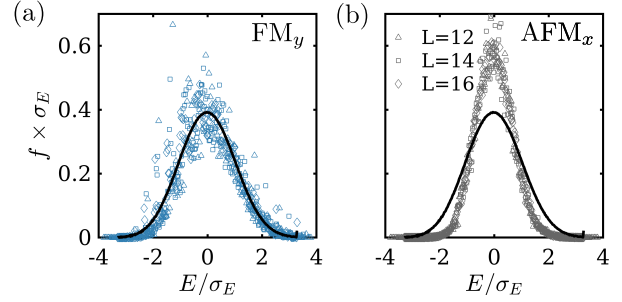


FIG. 3. Projection of the (a) FM_y and (b) AFM_x states on the eigenstate basis, $f(E) = \sum_n |\langle n | \Psi_0 \rangle|^2 \delta(E - \varepsilon_n)$, of the mixed field Ising model (MFIM), Eq. (28). In both panels, datapoints are shown for system sizes $L = 12$ (triangle), $L = 14$ (squares), and $L = 16$ (diamonds). Also shown with solid lines is the average projection of pure random states on the eigenstate basis.

V. ENSEMBLES EMERGING FROM CHAOTIC HAMILTONIAN DYNAMICS

A. Model

We consider the mixed field Ising model (MFIM),

$$H = \sum_j \hat{Z}_j \hat{Z}_{j+1} + g \hat{X}_j + h \hat{Z}_j, \quad (28)$$

which has been widely used as a canonical model of strongly chaotic dynamics [42, 73–75]. Here $\hat{X}_j, \hat{Y}_j, \hat{Z}_j$ denote the Pauli spin matrices, g is the transverse field, and h is the longitudinal field. The Hamiltonian (28) also has multiple point symmetries, which we explicitly break. In particular, we use open boundary conditions to break translation symmetry, and we include boundary fields $h_1 = \hat{Z}_1/4$ and $h_L = -\hat{Z}_L/4$ to break inversion symmetry. Of special interest in this work are the model parameters $(g, h) = (1.05, 0.35)$, which we have identified as the ‘most chaotic’ parameters in terms of eigenstate randomness [42], and are also close to the values used in many other works [73, 75].

To obtain the late-time ensemble, we first evolve the initial state $|\Psi_0\rangle$ (defined below) for long times $t \gg 1$ until the EE thermalizes. As before, we define the thermalization time as the time in which the average EE reaches its late-time value (within one standard deviation of the EE at late times). For all the system sizes $10 \leq L \leq 16$ and initial conditions considered in this work, we find that $t = 200$ is sufficient for the EE to thermalize. After thermalization, we draw 1000 states separated by timesteps $\Delta t = 0.1$.

B. Initial Conditions

Similarly to the $\text{U}(1)$ case, we consider two classes of mid-spectrum (zero energy) product state initial condi-

tions that have distinct late-time behavior. First, we consider the $|\text{FM}_y\rangle$ product state comprised of spins aligned in the y -axis. We find that the FM_y initial condition has a uniform projection on the Hamiltonian eigenstates, $|\langle n|\Psi_0\rangle| \sim 1/D$, and, as a result, satisfies the typicality condition (4). The spreading of $|\Psi_0\rangle$ on the eigenstate basis is shown in the histogram in Fig. 3(a) for $L = 12, 14, 16$. Second, we also consider the AFM_x initial comprised of spins antialigned in the x direction, which also has zero energy. Unlike the FM_y state, the AFM_x state is not uniformly distributed among eigenstates. In particular, the distribution has less energy variance than expected for a midspectrum product state, see Fig. 3(b). We emphasize that the smaller-than-typical-variance is not a finite-size effect, as the finite-size scaling plotted in Fig. 3(b) shows that the smaller energy variance persists in the thermodynamic limit.

For comparison, we also construct the analogue of the microcanonical ensemble Φ_M comprised of states with negligible energy variance, i.e., midspectrum eigenstates $\hat{H}|n\rangle = E_n|n\rangle$. More precisely, we define $\Phi_E = \{|n\rangle, E_n < |\epsilon|\}$, where $\epsilon \ll 1$ is a small parameter. To obtain the microcanonical ensemble, we first diagonalize the Hamiltonian (28), and then sample N_{mid} eigenstates in the middle of the spectrum to obtain Φ_E . We use $N_{\text{mid}} = 100, 300, 600, 1000$ midspectrum eigenstates for system sizes $L = 10, 12, 14, 16$, respectively.

C. Numerical Results

Figure 4(a) shows the late EE distribution for the FM_y (typical) and AFM_x (atypical) initial conditions, and the microcanonical EE distribution of midspectrum eigenstates (MC) for the MFIM with $(g, h) = (1.05, 0.35)$ and $L = 16$. We first emphasize the striking similarity between Figs. 4 and 2. On the one hand, the FM_y initial condition, which projects onto the eigenstate basis uniformly across eigenstates [Fig. 3(a)], exhibits an EE distribution that is indistinguishable from that of Haar random states, up to corrections that are exponentially small in system size. On the other hand, the AFM_x initial condition, with smaller-than-typical energy variance [Fig. 3(b)], leads to an EE distribution that is distinguishable from the Haar ensemble by several standard deviations. As discussed in Sec. IV, in the limiting case of negligible energy variance, the microcanonical EE distribution agrees with the $U(1)$ constrained RMT ensemble [left-most histogram in Fig. 4(a)], as first pointed out in Ref. [42].²

² Because the Hamiltonian has time-reversal symmetry, we sample Φ_M using real-values random states. This does not modify the mean EE, but its standard deviation increases by a factor of $\sqrt{2}$ [42, 76, 77]. This result is true both for constrained [42] and unconstrained ensembles [76, 77].

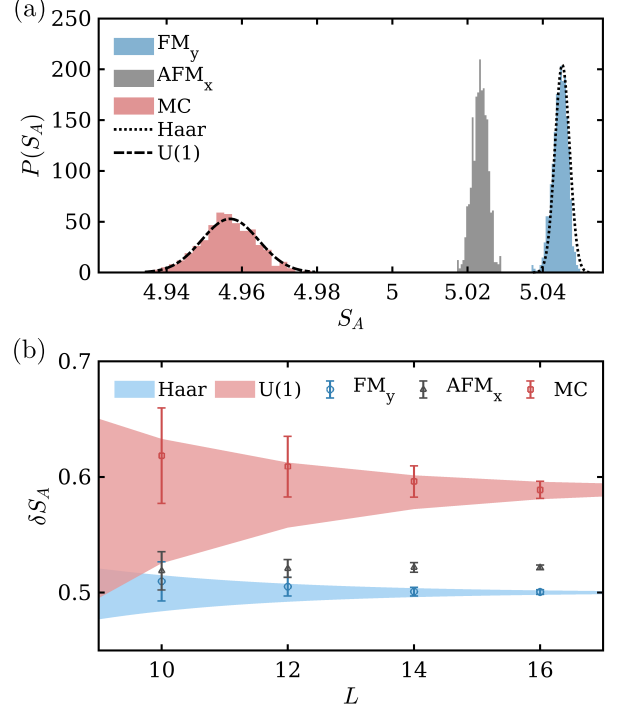


FIG. 4. (a) Distribution of EE at late times for the MFIM and different initial conditions. Also shown is the microcanonical distribution of EE for midspectrum eigenstates (MC). The dotted lines indicate the EE distribution of Haar random states, and the dotted-dashed lines indicate the EE distribution for states constrained to the $M = 0$ magnetic sector. (b) Finite-size scaling of the EE distributions plotted relative to the maximum EE value ($\delta S_A = L_A \log 2 - S_A$) for different initial conditions. The dots indicated the average EE value, and the bars indicated their standard deviation. The shaded areas indicates the regions limited by $S_A = \mu_H \pm \sigma_H$ (blue) and $S_A = \mu_M \pm \sigma_M$ (red) for the EE distribution of Haar and constrained random states, respectively.

Figure 4(b) shows the finite-size scaling behavior of panel (a), showing that the same behavior described above persists in the thermodynamic limit. Each datapoint represents the mean EE at late times for different system sizes L and initial conditions, and the bars represent the standard deviation of the EE distribution. For comparison, the shaded areas indicates the regions limited by $S_A = \mu_H \pm \sigma_H$ [Eq. (7)] and $S_A = \mu_M \pm \sigma_M$ [Eq. (11)] for the EE distribution of states within Φ_H and Φ_M ensembles, respectively. We find excellent convergence of all the distribution to their expected universal RMT behavior for the typical and the MC distributions. In addition, the atypical initial conditions remain distinguishable from Haar and microcanonical distributions for all system sizes.

So far, our results focused on the late-time behavior of typical and atypical initial states for maximally chaotic Hamiltonians. In particular, the numerical results for Fig. 4 were obtained for the most chaotic parameters $(g, h) = (1.05, 0.35)$ of the MFIM. We now show that the

main results are generic, i.e., the late-time ensemble of typical initial states are indistinguishable from Haar random states regardless of Hamiltonian details, so long as the Hamiltonian remains in the quantum chaotic regime. With this goal in mind, we use the same initial conditions (FM_y and AFM_x) in the MFIM and tune the value of g away from maximal chaos. As shown in Fig. 5(a), the late-time EE distribution for the typical (FM_y) initial condition approaches the EE distribution of Haar random states for a broad range of g values between $0.5 \lesssim g \lesssim 2$. In addition, the finite-scaling of the results in Fig. 5(b) shows that the range of g 's in which the late-time EE distribution approaches the Haar ensemble increases with system size. This suggests that, in the thermodynamic limit, the late-time distribution of quantum states becomes indistinguishable from Haar random states for all values of g so long as the Hamiltonian is quantum chaotic (i.e., $g \neq 0$).

The behavior is qualitatively distinct for atypical initial states (FM_x), as these exhibit a strong sensitivity to the Hamiltonian parameters, as shown in Fig. 5(a). This behavior is analogous to that shown in Fig. 2(b) for spin spiral states, where we found that details of the initial condition modify the late-time behavior of quantum states, and such finer finer can be distinguished through $O(1)$ corrections to the EE.

Finally, we comment on the behavior of the microcanonical eigenstate ensemble Φ_E across model parameters. As shown in Fig. 5(a), the microcanonical ensemble exhibits a wide range of variability of EE as a function of g (unlike the behavior of the late-time ensembles), and reaches the constrained RMT behavior [$U(1)$] at the ‘most chaotic’ parameters centered around $g = 1.05$. This behavior was studied in more detail in a previous work [42] by one of us. In a nutshell, this behavior can be understood by noticing that eigenstates have much more structure than time-evolved states and, as a result, are less entropic. This is because spatial locality is strongly imprinted in the structure of eigenstates, whereas spatial locality is effectively washed away during evolution at late-times (for this reason, one can reconstruct the full Hamiltonian from a generic eigenstate if the Hamiltonian is local [78, 79]). Only at the ‘maximally chaotic’ parameters eigenstates are maximally entropic and have spatial locality and energy conservation as their only features; everywhere else in parameters space, particularly as system approach integrable limits, the microcanonical eigenstate ensemble contains additional structure and, as a result, lower EE.

VI. SUMMARY AND DISCUSSION

Our work has shown that quantum states undergoing strongly chaotic dynamics in the presence of symmetries can exhibit rich classes of dynamical behaviors at late times, even if the states lies in middle of the spectrum. These rich behaviors emerge when studying higher sta-

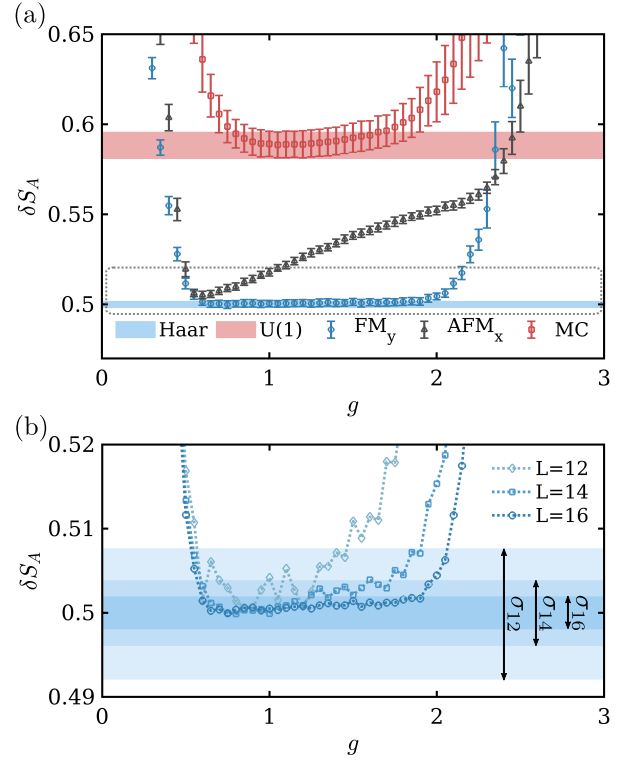


FIG. 5. (a) Distribution of EE at late-times for the MFIM as a function of the transverse field g and initial conditions (FM_y and AFM_x). Also shown is the EE distribution of the microcanonical eigenstate ensemble (MC). All values are plotted relative to the maximum EE ($\delta S_A = L_A \log 2 - S_A$). The symbols indicate the average EE value for each value of g , and the bars indicate their standard deviation. The shaded areas indicates the regions limited by $S_A = \mu \pm \sigma$ (blue) and $S_A = \mu_M \pm \sigma_M$ (red) for the EE distribution of Haar and constrained random states, respectively. (b) Zoom of the dotted region in panel (a) for the FM_y initial condition showing EE data for different system sizes $L = 12, 14, 16$. The width σ_L of the shaded regions indicate the standard deviation of the EE for the different system sizes.

tistical moments of the quantum state ensembles, particularly the universal behavior of state-to-state fluctuations at late times, and beyond the widely-studied coarse-grained behaviors, such as the volume-law behavior of the entanglement entropy.

In a nutshell, our work has identified two limiting regimes for the late-time ensemble which exhibit universality at the level of higher statistical moments. In one limit, *typical* initial states effectively mix symmetry sectors in such a way that finite k -moments of the late-time ensemble exactly agree with Haar random states in the thermodynamic limit, i.e., no measurement can be done to tell that the late-time ensemble of typical initial states is not exploring all of phase space. For finite-sized systems, it is exponentially hard to tell both ensembles apart. This result is quite striking, as the ensemble of quantum states at late-time do not explore the entire Hilbert space when evolution is constrained by symme-

tries. In the opposite limit, states with negligible variance of the symmetry operator also acquire universal behavior which can be described by pure random state ensembles constrained to the corresponding symmetry sector of the symmetry operator. Both limiting ensembles can be distinguished by measuring subsystem properties, without the need to access the full quantum state. Initial states that lie in between both limiting regimes exhibit late-time dynamics which agrees with the Haar ensemble only at the level of average coarse-grained behavior, but their higher statistical moments are non-universal.

In addition to characterizing the universal structure of late-time ensembles in quantum chaotic systems, we also emphasize several ramifications of our work. The first ramification relates to our understanding of quantum chaos. The widely-accepted definition of quantum chaos is rooted in the RMT behavior of Hamiltonian eigenspectrum and eigenstates [28–36, 38, 39]. As we argued above, this definition only captures the average coarse-grained behavior and applies generically to any Hamiltonian away from integrable limits. When looking at higher statistical moments, our work finds qualitatively distinct differences between eigenstate ensembles and late-time ensembles. On the one hand, local Hamiltonian systems exhibit a large degree of universality—at the level of higher moments—in the late-time ensemble of typical initial conditions regardless of microscopic details of the Hamiltonian [Fig. 5]. In contrast, eigenstate ensembles exhibit a much rich landscape of behaviors, with higher moments of the eigenstate ensembles agreeing with constrained RMT ensemble only in small pockets of parameter space—the ‘maximally chaotic’ parameters (see also Ref. [42]). The key distinction between both ensembles is the role of spatial locality: whereas spatial locality is imprinted in the structure of eigenstates, spatial locality is washed away during dynamics at late times. The higher statistical moments of the quantum state ensembles can tell such differences apart. An interesting direction for future work is creating sharper definitions of quantum chaos that account for higher statistical moments of quantum states, both at the level of eigenstates and temporal ensembles.

A second ramification of our work relates to randomization of quantum information in quantum devices. Modern experimental platforms operate under a large number of constraints, including spatial locality (gates operate between neighboring qubits) and a restricted subset of local gates [12–19]. This raises questions about how much randomness a quantum device can generate [12, 14, 20]. Our results suggest that even when quantum evolution is constrained by locality and simple symmetries such that not *all* states are generated during evolution, one can still get a late-time ensemble that essentially is indistinguishable from the Haar distribution if initial conditions are properly chosen. Generalizing our results to more complex constraints is an interesting direction for future research.

A third ramification relates to the existence of atypi-

cal midspectrum initial conditions that exhibit smaller-than-typical entanglement entropy at late times. Although midspectrum states with smaller-than-typical entanglement are reminiscent of many-body quantum scars [80, 81], we emphasize that quantum scars have anomalously small entanglement entropy due to the absence of volume law behavior, whereas the atypical states discussed here still have volume law behavior but smaller-than-typical EE at the level of $O(1)$ corrections and statistical fluctuations. Also, quantum scars are fine-tuned and require special phase space structure of the Hamiltonian [82], possibly proximity to integrability [83], whereas the atypical states discussed here are robust and ubiquitous, persisting irrespective of the Hamiltonian details (Fig. 5). Understanding in more detail the dynamic and thermalizing properties of these atypical states is another interesting direction for future research.

ACKNOWLEDGEMENTS

We thank Wen Wei Ho and Shenglong Xu for insightful discussions, and Vedika Khemani for previous collaborations. JFRN acknowledges the hospitality of the Aspen Center for Physics, which is supported by National Science Foundation grant PHY-2210452, and a grant from the Alfred P. Sloan Foundation (G-2024-22395). The numerical simulations in this work were conducted with the advanced computing resources provided by Texas A&M High Performance Research Computing.

Appendix A: Trace distance between Haar random states and typical random states

To compute the trace distance between the second moment of the ensemble of Haar random states, Eq.(8), and the ensemble of typical random states, Eqs.(12) and (13), we first note that the matrix $\delta\rho^{(k=2)}$ is a sparse matrix that has non-zero off-diagonal entries only for permutations of the $m_1 \neq m_2$ indeces, i.e., $\delta\rho_{m_1 m_2, m_2 m_1}^{(k=2)} \neq 0$. To diagonalize this sparse matrix, we use the basis $|M, \alpha\rangle$ of the Z operator used in Eqs.(12)–(13). We consider three distinct cases.

(i) When $M_1 \neq M_2$, there is a total of $\sum_{M_1 \neq M_2} D_{M_1} D_{M_2}$ terms that contribute to the trace distance. Each state $(M_1 \alpha_1, M_2 \alpha_2)$ is coupled to the state obtained by permuting its indeces, $(M_2 \alpha_2, M_1 \alpha_1)$, and the eigenvalues of the two-by-two matrix describing this subspace are 0 and $\frac{1}{D^2} - \frac{1}{D^2(1+1/D)}$. We also note that $\sum_{M_1 \neq M_2} D_{M_1} D_{M_2} = \sum_{M_1 M_2} D_{M_1} D_{M_2} - \sum_M D_M^2 = D^2 - \sum_M D_M^2$.

(ii) When $M_1 = M_2 = M$ and $\alpha_1 \neq \alpha_2$, for each symmetry sector M there is a total of $D_M(D_M - 1)$ terms that contribute to the trace distance. Each state $(M \alpha_1, M \alpha_2)$ is only coupled to the state obtained by permuting its indeces, $(M \alpha_2, M \alpha_1)$, and the eigenvalues of

the two-by-two matrix describing this subspace are 0 and $\frac{1}{D^2(1+1/D)} - \frac{1}{D^2(1+1/D_M)}$.

(iii) When $M_1 = M_2 = M$ and $\alpha_1 = \alpha_2$, there is a total of D_M terms that contribute to the trace distance in each symmetry sector M . Each term contributes $\frac{1}{D^2(1+1/D_M)} - \frac{1}{D^2(1+1/D)}$ to the trace distance.

Combining all three contributions (i)-(iii), the trace distance is given by

$$\begin{aligned} \Delta_{k=2} = & \frac{1}{2} \left(1 - \frac{1}{D^2} \sum_M D_M^2 \right) \left(1 - \frac{1}{1+1/D} \right) \\ & + \sum_M \frac{D_M(D_M-1)}{2D^2} \left(\frac{1}{1+1/D} - \frac{1}{1+1/D_M} \right) \\ & + \sum_M \frac{D_M}{D^2} \left(\frac{1}{1+1/D_M} - \frac{1}{1+1/D} \right). \end{aligned} \quad (\text{A1})$$

We next expand Eq. (A1) up to order $\mathcal{O}(1/D^2)$. The term in the first line of the right-hand-side is

$$\left(1 - \frac{1}{D^2} \sum_M D_M^2 \right) \left(1 - \frac{1}{1+1/D} \right) \approx \frac{1}{D} \left(1 - \frac{1}{\sqrt{\pi L}} \right), \quad (\text{A2})$$

where we used the equality $\sum_M D_M^2 = \sum_{M=0}^L \binom{L}{M}^2 = \binom{2L}{L}$, combined with Stirling's approximation $\binom{2L}{L} \approx \frac{2^{2L}}{\sqrt{\pi L}} = \frac{D^2}{\sqrt{\pi L}}$. Second, we combine all the terms that have denominator $\frac{1}{1+1/D}$ in the second and third lines of Eq. (A1). This gives

$$\begin{aligned} \sum_M \frac{D_M(D_M-3)}{D^2(1+1/D)} & \approx \left(\frac{1}{\sqrt{\pi L}} - \frac{3}{D} \right) \left(1 - \frac{1}{D} \right) \\ & = \left(\frac{1}{\sqrt{\pi L}} - \frac{3}{D} - \frac{1}{D\sqrt{\pi L}} \right), \end{aligned} \quad (\text{A3})$$

where we used again the approximation $\sum_M D_M^2 \approx \frac{D^2}{\sqrt{\pi L}}$. Third, we combine all the terms that have denominator $\frac{1}{D^2(1+D_M^{-1})}$ in the second and third lines of Eq. (A1). This gives

$$\begin{aligned} \sum_M \frac{D_M(D_M-3)}{D^2(1+D_M^{-1})} & = \sum_M \frac{D_M(D_M-3)}{D^2} \left(1 - \frac{1}{D_M} + \dots \right) \\ & \approx \sum_M \frac{D_M^2 - 4D_M}{D^2} = \left(\frac{1}{\sqrt{\pi L}} - 4D \right) \end{aligned} \quad (\text{A4})$$

By summing all the terms in Eqs. (A2)-(A4), we obtain Eq. (14) in the main text.

[1] J. M. Deutsch, "Quantum statistical mechanics in a closed system," *Phys. Rev. A* **43**, 2046–2049 (1991).

[2] Mark Srednicki, "Chaos and quantum thermalization," *Phys. Rev. E* **50**, 888–901 (1994).

[3] Mark Srednicki, "The approach to thermal equilibrium in quantized chaotic systems," *Journal of Physics A: Mathematical and General* **32**, 1163–1175 (1999).

[4] Marcos Rigol, Vanja Dunjko, and Maxim Olshanii, "Thermalization and its mechanism for generic isolated quantum systems," *Nature* **452**, 854–858 (2008).

[5] Luca D'Alessio, Yariv Kafri, Anatoli Polkovnikov, and Marcos Rigol, "From quantum chaos and eigenstate thermalization to statistical mechanics and thermodynamics," *Advances in Physics* **65**, 239–362 (2016).

[6] Joshua M Deutsch, "Eigenstate thermalization hypothesis," *Reports on Progress in Physics* **81**, 082001 (2018).

[7] Arnau Riera, Christian Gogolin, and Jens Eisert, "Thermalization in nature and on a quantum computer," *Phys. Rev. Lett.* **108**, 080402 (2012).

[8] Christian Gogolin and Jens Eisert, "Equilibration, thermalisation, and the emergence of statistical mechanics in closed quantum systems," *Reports on Progress in Physics* **79**, 056001 (2016).

[9] Daniel K. Mark, Federica Surace, Andreas Elben, Adam L. Shaw, Joonhee Choi, Gil Refael, Manuel Endres, and Soonwon Choi, "A maximum entropy principle in deep thermalization and in hilbert-space ergodicity," (2024).

[10] Noah Linden, Sandu Popescu, Anthony J. Short, and Andreas Winter, "Quantum mechanical evolution towards thermal equilibrium," *Phys. Rev. E* **79**, 061103 (2009).

[11] Yoshifumi Nakata, Peter S. Turner, and Mio Murao, "Phase-random states: Ensembles of states with fixed amplitudes and uniformly distributed phases in a fixed basis," *Phys. Rev. A* **86**, 012301 (2012).

[12] Google Team and Collaborators, "Quantum supremacy using a programmable superconducting processor," *Nature* **574**, 505–510 (2019).

[13] Google Team and Collaborators, "Dynamics of magnetization at infinite temperature in a Heisenberg spin chain," *Science* **384**, 48–53 (2024).

[14] Google Team and Collaborators, "Information scrambling in quantum circuits," *Science* **374**, 1479–1483 (2021).

[15] Hannes Bernien, Sylvain Schwartz, Alexander Keesling, Harry Levine, Ahmed Omran, Hannes Pichler, Soonwon Choi, Alexander S. Zibrov, Manuel Endres, Markus Greiner, Vladan Vuletić, and Mikhail D. Lukin, "Probing many-body dynamics on a 51-atom quantum simulator," *Nature* **551**, 579–584 (2017).

[16] Sepehr Ebadi, Tout T. Wang, Harry Levine, Alexander Keesling, Giulia Semeghini, Ahmed Omran, Dolev Bluvstein, Rhine Samajdar, Hannes Pichler, Wen Wei Ho, Soonwon Choi, Subir Sachdev, Markus Greiner, Vladan Vuletić, and Mikhail D. Lukin, "Quantum phases of matter on a 256-atom programmable quantum simulator," *Nature* **595**, 227–232 (2021).

[17] Pascal Scholl, Michael Schuler, Hannah J. Williams, Alexander A. Eberharter, Daniel Barredo, Kai-

Niklas Schymik, Vincent Lienhard, Louis-Paul Henry, Thomas C. Lang, Thierry Lahaye, Andreas M. Läuchli, and Antoine Browaeys, “Quantum simulation of 2D antiferromagnets with hundreds of rydberg atoms,” *Nature* **595**, 233–238 (2021).

[18] J. Zhang, G. Pagano, P. W. Hess, A. Kyprianidis, P. Becker, H. Kaplan, A. V. Gorshkov, Z.-X. Gong, and C. Monroe, “Observation of a many-body dynamical phase transition with a 53-qubit quantum simulator,” *Nature* **551**, 601–604 (2017).

[19] C. Monroe, W. C. Campbell, L.-M. Duan, Z.-X. Gong, A. V. Gorshkov, P. W. Hess, R. Islam, K. Kim, N. M. Linke, G. Pagano, P. Richerme, C. Senko, and N. Y. Yao, “Programmable quantum simulations of spin systems with trapped ions,” *Rev. Mod. Phys.* **93**, 025001 (2021).

[20] Joonhee Choi, Adam L. Shaw, Ivaylo S. Madjarov, Xin Xie, Ran Finkelstein, Jacob P. Covey, Jordan S. Cotler, Daniel K. Mark, Hsin-Yuan Huang, Anant Kale, Hannes Pichler, Fernando G. S. L. Brandão, Soonwon Choi, and Manuel Endres, “Preparing random states and benchmarking with many-body quantum chaos,” *Nature* **613**, 468–473 (2023).

[21] Ewan McCulloch, Jacopo De Nardis, Sarang Gopalakrishnan, and Romain Vasseur, “Full counting statistics of charge in chaotic many-body quantum systems,” *Phys. Rev. Lett.* **131**, 210402 (2023).

[22] Sarang Gopalakrishnan, Alan Morningstar, Romain Vasseur, and Vedika Khemani, “Distinct universality classes of diffusive transport from full counting statistics,” *Phys. Rev. B* **109**, 024417 (2024).

[23] Alexander Lukin, Matthew Rispoli, Robert Schittko, M. Eric Tai, Adam M. Kaufman, Soonwon Choi, Vedika Khemani, Julian Léonard, and Markus Greiner, “Probing entanglement in a many-body localized system,” *Science* **364**, 256–260 (2019).

[24] A. Elben, B. Vermersch, M. Dalmonte, J. I. Cirac, and P. Zoller, “Rényi entropies from random quenches in atomic hubbard and spin models,” *Phys. Rev. Lett.* **120**, 050406 (2018).

[25] Tiff Brydges, Andreas Elben, Petar Jurcevic, Benoît Vermersch, Christine Maier, Ben P. Lanyon, Peter Zoller, Rainer Blatt, and Christian F. Roos, “Probing renyi entanglement entropy via randomized measurements,” *Science* **364**, 260–263 (2019).

[26] Andreas Elben, Steven T. Flammia, Hsin-Yuan Huang, Richard Kueng, John Preskill, Benoît Vermersch, and Peter Zoller, “The randomized measurement toolbox,” *Nature Reviews Physics* **5**, 9–24 (2023).

[27] Madan Lal Mehta, *Random Matrices*, 3rd ed. (2004).

[28] Y Y Atas, E Bogomolny, O Giraud, P Vivo, and E Vivo, “Joint probability densities of level spacing ratios in random matrices,” *Journal of Physics A: Mathematical and Theoretical* **46**, 355204 (2013).

[29] Y. Y. Atas, E. Bogomolny, O. Giraud, and G. Roux, “The distribution of the ratio of consecutive level spacings in random matrix ensembles,” *Phys. Rev. Lett.* **110**, 084101 (2013).

[30] Vadim Oganesyan and David A. Huse, “Localization of interacting fermions at high temperature,” *Phys. Rev. B* **75**, 155111 (2007).

[31] Bruno Bertini, Pavel Kos, and Tomaz Prosen, “Exact spectral form factor in a minimal model of many-body quantum chaos,” *Phys. Rev. Lett.* **121**, 264101 (2018).

[32] Pavel Kos, Marko Ljubotina, and Tomaz Prosen, “Many-body quantum chaos: Analytic connection to random matrix theory,” *Phys. Rev. X* **8**, 021062 (2018).

[33] Amos Chan, Andrea De Luca, and J. T. Chalker, “Solution of a minimal model for many-body quantum chaos,” *Phys. Rev. X* **8**, 041019 (2018).

[34] Dibyendu Roy and Tomaz Prosen, “Random matrix spectral form factor in kicked interacting fermionic chains,” *Phys. Rev. E* **102**, 060202 (2020).

[35] Chaitanya Murthy and Mark Srednicki, “Structure of chaotic eigenstates and their entanglement entropy,” *Phys. Rev. E* **100**, 022131 (2019).

[36] Tsung-Cheng Lu and Tarun Grover, “Renyi entropy of chaotic eigenstates,” *Phys. Rev. E* **99**, 032111 (2019).

[37] Lev Vidmar and Marcos Rigol, “Entanglement entropy of eigenstates of quantum chaotic hamiltonians,” *Phys. Rev. Lett.* **119**, 220603 (2017).

[38] M. Kliczkowski, R. Swietek, L. Vidmar, and M. Rigol, “Average entanglement entropy of midspectrum eigenstates of quantum-chaotic interacting hamiltonians,” *Phys. Rev. E* **107**, 064119 (2023).

[39] Eugenio Bianchi, Lucas Hackl, Mario Kieburg, Marcos Rigol, and Lev Vidmar, “Volume-law entanglement entropy of typical pure quantum states,” *PRX Quantum* **3**, 030201 (2022).

[40] Yichen Huang, “Universal entanglement of mid-spectrum eigenstates of chaotic local hamiltonians,” *Nuclear Physics B* **966**, 115373 (2021).

[41] Masudul Haque, Paul A. McClarty, and Ivan M. Khaymovich, “Entanglement of midspectrum eigenstates of chaotic many-body systems: Reasons for deviation from random ensembles,” *Phys. Rev. E* **105**, 014109 (2022).

[42] Joaquin F. Rodriguez-Nieva, Cheryne Jonay, and Vedika Khemani, “Quantifying quantum chaos through micro-canonical distributions of entanglement,” *Phys. Rev. X* **14**, 031014 (2024).

[43] Christopher M. Langlett and Joaquin F. Rodriguez-Nieva, “Entanglement patterns of quantum chaotic hamiltonians with a scalar U(1) charge,” (2024).

[44] Amos Chan, Andrea De Luca, and J. T. Chalker, “Eigenstate correlations, thermalization, and the butterfly effect,” *Phys. Rev. Lett.* **122**, 220601 (2019).

[45] Laura Foini and Jorge Kurchan, “Eigenstate thermalization hypothesis and out of time order correlators,” *Phys. Rev. E* **99**, 042139 (2019).

[46] Jonas Richter, Anatoly Dymarsky, Robin Steinigeweg, and Jochen Gemmer, “Eigenstate thermalization hypothesis beyond standard indicators: Emergence of random-matrix behavior at small frequencies,” *Phys. Rev. E* **102**, 042127 (2020).

[47] S. J. Garratt and J. T. Chalker, “Local pairing of feynman histories in many-body floquet models,” *Phys. Rev. X* **11**, 021051 (2021).

[48] Jiaozi Wang, Mats H. Lamann, Jonas Richter, Robin Steinigeweg, Anatoly Dymarsky, and Jochen Gemmer, “Eigenstate thermalization hypothesis and its deviations from random-matrix theory beyond the thermalization time,” *Phys. Rev. Lett.* **128**, 180601 (2022).

[49] Marlon Brener, Silvia Pappalardi, Mark T. Mitchison, John Goold, and Alessandro Silva, “Out-of-time-order correlations and the fine structure of eigenstate thermalization,” *Phys. Rev. E* **104**, 034120 (2021).

[50] Jordan S. Cotler, Daniel K. Mark, Hsin-Yuan Huang, Felipe Hernandez, Joonhee Choi, Adam L. Shaw, Manuel

Endres, and Soonwon Choi, “Emergent quantum state designs from individual many-body wavefunctions,” *PRX Quantum* **4**, 010311 (2023).

[51] Wen Wei Ho and Soonwon Choi, “Exact emergent quantum state designs from quantum chaotic dynamics,” *Phys. Rev. Lett.* **128**, 060601 (2022).

[52] Matteo Ippoliti and Wen Wei Ho, “Solvable model of deep thermalization with distinct design times,” *Quantum* **6**, 886 (2022).

[53] Maxime Lucas, Lorenzo Piroli, Jacopo De Nardis, and Andrea De Luca, “Generalized deep thermalization for free fermions,” *Physical Review A* **107**, 032215 (2023).

[54] Saul Pilatowsky-Cameo, Ceren B. Dag, Wen Wei Ho, and Soonwon Choi, “Complete Hilbert-Space Ergodicity in Quantum Dynamics of Generalized Fibonacci Drives,” *Physical Review Letters* **131**, 250401 (2023).

[55] Nicholas Hunter-Jones, “Unitary designs from statistical mechanics in random quantum circuits,” (2019), [arXiv:1905.12053](https://arxiv.org/abs/1905.12053).

[56] Daniel A. Roberts and Beni Yoshida, “Chaos and complexity by design,” *Journal of High Energy Physics* **2017**, 1–64 (2017).

[57] Michele Fava, Jorge Kurchan, and Silvia Pappalardi, “Designs via Free Probability,” (2023), [10.48550/arXiv.2308.06200](https://arxiv.org/abs/2308.06200).

[58] Silvia Pappalardi, Felix Fritzsch, and Tomaz Prosen, “General Eigenstate Thermalization via Free Cumulants in Quantum Lattice Systems,” (2023), [10.48550/arXiv.2303.00713](https://arxiv.org/abs/2303.00713).

[59] Kazuya Kaneko, Eiki Iyoda, and Takahiro Sagawa, “Characterizing complexity of many-body quantum dynamics by higher-order eigenstate thermalization,” *Phys. Rev. A* **101**, 042126 (2020).

[60] Don N. Page, “Average entropy of a subsystem,” *Phys. Rev. Lett.* **71**, 1291–1294 (1993).

[61] Aram W. Harrow, “The church of the symmetric subspace,” (2013), [arXiv:1308.6595 \[quant-ph\]](https://arxiv.org/abs/1308.6595).

[62] Liangsheng Zhang, Hyungwon Kim, and David A. Huse, “Thermalization of entanglement,” *Phys. Rev. E* **91**, 062128 (2015).

[63] Po-Yao Chang, Xiao Chen, Sarang Gopalakrishnan, and J. H. Pixley, “Evolution of entanglement spectra under generic quantum dynamics,” *Phys. Rev. Lett.* **123**, 190602 (2019).

[64] Bruno Bertini and Pasquale Calabrese, “Prethermalization and thermalization in entanglement dynamics,” *Phys. Rev. B* **102**, 094303 (2020).

[65] Jordan Cotler, Nicholas Hunter-Jones, and Daniel Ranard, “Fluctuations of subsystem entropies at late times,” *Phys. Rev. A* **105**, 022416 (2022).

[66] Bruno Bertini, Pavel Kos, and Tomaz Prosen, “Entanglement spreading in a minimal model of maximal many-body quantum chaos,” *Phys. Rev. X* **9**, 021033 (2019).

[67] Jas Bensa and Marko Žnidarič, “Fastest local entanglement scrambler, multistage thermalization, and a non-hermitian phantom,” *Phys. Rev. X* **11**, 031019 (2021).

[68] Eugenio Bianchi and Pietro Donà, “Typical entanglement entropy in the presence of a center: Page curve and its variance,” *Phys. Rev. D* **100**, 105010 (2019).

[69] Pierpaolo Vivo, Mauricio P. Pato, and Gleb Oshanin, “Random pure states: Quantifying bipartite entanglement beyond the linear statistics,” *Phys. Rev. E* **93**, 052106 (2016).

[70] Lu Wei, “Proof of vivo-pato-oshanin’s conjecture on the fluctuation of von neumann entropy,” *Phys. Rev. E* **96**, 022106 (2017).

[71] Matthew P.A. Fisher, Vedika Khemani, Adam Nahum, and Sagar Vijay, “Random quantum circuits,” *Annual Review of Condensed Matter Physics* **14**, 335–379 (2023).

[72] Cheryne Jonay, Joaquin F. Rodriguez-Nieva, and Vedika Khemani, “Slow thermalization and subdiffusion in U(1) conserving floquet random circuits,” *Phys. Rev. B* **109**, 024311 (2024).

[73] M. C. Bañuls, J. I. Cirac, and M. B. Hastings, “Strong and weak thermalization of infinite nonintegrable quantum systems,” *Phys. Rev. Lett.* **106**, 050405 (2011).

[74] Hyungwon Kim and David A. Huse, “Ballistic spreading of entanglement in a diffusive nonintegrable system,” *Phys. Rev. Lett.* **111**, 127205 (2013).

[75] Daniel E. Parker, Xiangyu Cao, Alexander Avdoshkin, Thomas Scaffidi, and Ehud Altman, “A universal operator growth hypothesis,” *Phys. Rev. X* **9**, 041017 (2019).

[76] Pierpaolo Vivo, “Entangled random pure states with orthogonal symmetry: exact results,” *Journal of Physics A: Mathematical and Theoretical* **43**, 405206 (2010).

[77] Santosh Kumar and Akhilesh Pandey, “Entanglement in random pure states: spectral density and average von neumann entropy,” *Journal of Physics A: Mathematical and Theoretical* **44**, 445301 (2011).

[78] James R. Garrison and Tarun Grover, “Does a single eigenstate encode the full hamiltonian?” *Phys. Rev. X* **8**, 021026 (2018).

[79] Xiao-Liang Qi and Daniel Ranard, “Determining a local Hamiltonian from a single eigenstate,” *Quantum* **3**, 159 (2019).

[80] C. J. Turner, A. A. Michailidis, D. A. Abanin, M. Serbyn, and Z. Papić, “Weak ergodicity breaking from quantum many-body scars,” *Nature Physics* **14**, 745–749 (2018).

[81] Maksym Serbyn, Dmitry A. Abanin, and Zlatko Papić, “Quantum many-body scars and weak breaking of ergodicity,” *Nature Physics* **17**, 675 (2021).

[82] Anushya Chandran, Thomas Iadecola, Vedika Khemani, and Roderich Moessner, “Quantum many-body scars: A quasiparticle perspective,” *Annual Review of Condensed Matter Physics* **14**, 443–469 (2023).

[83] Vedika Khemani, Chris R. Laumann, and Anushya Chandran, “Signatures of integrability in the dynamics of rydberg-blockaded chains,” *Phys. Rev. B* **99**, 161101 (2019).